RADIATION SAFETY IN AIRCRAFT OPERATIONS

ICAS-92-5.3.4

J. W. Wilson and J. E. Nealy
Space Systems Division
NASA Langley Research Center
Hampton, VA 23665-5225

Abstract

The impact of radiation on proposed high-altitude aircraft received considerable attention at the Langley Research Center following the proposal for development of a commercial supersonic transport. Although subsonic operations were at that time considered to be of negligible radiation risk, several factors have changed since those early studies which greatly increase risk estimates to subsonic aircraft crews. These factors include: (1) higher altitudes used to increase fuel efficiency and reduce air-traffic density; (2) United States flight crews have doubled their flight hours since deregulation; (3) estimates of the relative effectiveness of neutrons for biological injury are much greater than previously assumed; and (4) the excess cancer risk coefficients for low-level exposure are found to be substantially larger than previously estimated. A 7-year flight experiment program was conducted to measure the significant biological components (tissue ionization rates, neutron flux, and nuclear reaction star rates) as a function of solar cycle, altitude, latitude, and longitude from which biological risk is estimated. This atmospheric radiation data base is used in this paper to evaluate dose and dose equivalent along specific flight trajectories and agrees well with measurements. It is now well established that many current commercial flight paths would give exposures significantly greater than that allowed for the general public. Although the crews are not considered radiation workers in the usual sense of this classification, they remain one of the most highly exposed occupational groups. Dose equivalent rate along a New York to Tokyo flight at a 40,000-ft. altitude yields a career dose for approximately 1000 flight hours per year of 0.35 Sv and gives an excess cancer risk of 0.6 percent. A pregnant crew member would exceed recommended limits for prenatal exposure of 5 mSv during gestation. Potential use of this atmospheric radiation model for crew counseling and alternate flight assignments will be discussed.

Introduction

Recent interest in exposure and incurred dose due to ionizing radiation along commercial airlanes (upper troposphere and stratosphere) is due to several factors: increasing awareness of latent carcinogenic effects as a result of cumulative exposure;[1,2] newly proposed quality factors based on recent statistical studies and biological effects measurements;[2] and growing sophistication of aircraft microelectronic systems and controls which are susceptible to deleterious effects from high-energy heavy ions and nucleons.[3] The background radiation, which is due to interaction of the galactic cosmic rays (GCR) with the Earth's atmosphere, exhibits both temporal and spatial intensity variations. A series of experimental measurements and associated studies conducted at the NASA Langley Research Center[4] during portions of solar cycles XIX and XX has been utilized in the formulation of a data base for characterization of background radiation levels throughout the atmosphere as a function of time. These experiments were performed on instrumented aircraft (over 300 flights) and high-altitude balloons (25 flights). The experimental apparatus included liquid scintillation detectors for neutron spectral measurements, tissue-equivalent ion chambers for recording dose rate, and nuclear emulsion plates providing information on the high linear energy transfer (LET) constituents. In addition to measurement of solar cycle modulation effects and solar cosmic ray events, rather complete surveys of intensity variation with latitude and altitude were performed.

The dependence on altitude relates most directly to the local pressure or quantity of atmosphere available for interaction and attenuation. Latitudinal effects are principally due to the influence of the geomagnetic field; longitudinal variations also result from the asymmetry of this field. Seasonal influences arise as a result of the changes in pressure at a given altitude; winter-to-summer pressure variations have been observed to be somewhat greater in the Northern Hemisphere, for which the climatology is more complex. Orographic features, to a lesser extent, also influence the altitude variation of observed intensity. This extensive and comprehensive data base provides sufficient information for detailed modeling of these phenomena.

A permanent file data base consisting of the derived dose response functions has been incorporated into an algorithm formulated to compute a predicted dose rate along prescribed flight paths. Variations within the solar cycle are expressed in terms of ground-level neutron monitor count rates. These count rates are greatest during solar minimum, or quiet Sun, conditions when GCR flux is highest. With regard to geomagnetic influence, the dose and flux measurements have been correlated with recent, detailed, vertical cutoff rigidity data. Seasonal dependence and other factors influencing variation with geographic location (e.g., North-South Hemisphere asymmetry due to orography) have been modeled by incorporating climatological data obtained from the Langley 3-D Global General Circulation Model. Calculation of dose-equivalent rates may be performed in terms of the present (ICRP 26) quality factors[5] or recently recommended (ICRP 60) values.[2]

Efforts have been made to make the code in its present version computationally efficient, user-friendly, and readily adaptable to modification for special applications. In its present form, each case requires origin and destination latitudes and longitudes, calendar date, solar activity index (neutron monitor count rate), and altitude of flight path. Computation of dose-equivalent rate as a function of location along the flight path, and an average dose rate for the flight, are computed in 1 or 2 seconds. The FORTRAN code is available in versions compatible with either mainframes or personal computers. In the present note we will give a brief description of the data base used and the corresponding time dependent global model.

Flight Experimental Program

The flight experimental package consisted of encapsulated NE-218 and NE-222 organic liquid scintillators for neutron spectral measurements throughout the fast spectral region and above, tissue equivalent ion chambers, and nuclear emulsion. The tissue equivalent ion chamber measures the overall radiation dose while the neutron spectrometer and nuclear emulsion allow assessment of high LET components. The light generated in the scintillator by neutrons is mostly through high LET elastic recoil protons and neutron induced nuclear reactions. The light pulse generated by photons and high energy charged particles are low LET events and have a different pulse shape than the high LET neutron events. The Daehnick and Sherr[6] pulse shape discrimination technique was used to detect neutron pulses. The neutron rejection ratio was measured by Korff et al.[7] to be 1 in 10^4. The neutron pulses were analyzed in seven channels. The channel response functions were calculated using the computer program of Kurz[8] and calibrated with monoenergetic neutrons at the Oak Ridge National Laboratory using p + ^{3}H, ^{2}H + ^{2}H and ^{3}H + ^{1}H reactions. Further calibration was with Am - Be sources for testing stability before and after flights. The uncertainty in the detector response is about 10 percent.[7] The two inch and 6 inch diameter tissue equivalent ion chambers were built to the design specifications of M.F. Schneider[9] of the Air Force Weapons Laboratory for the Apollo space program. The detector wall was constructed of Shonka plastic and the filling gas was a mixture of CH_4, CO_2 and N_2 in proportions to approximate soft tissue. The six inch spherical chamber was sensitive to 0.1 μGy h^{-1}. The system response was shown stable over a very broad temperature range.[10] The system was calibrated using 30 to 155 MeV protons and ^{137}Cs sources. Ilford G5 nuclear emulsion in sufficient quantity for good statistics was used to measure the nuclear star rates in tissue.

The extent of the NASA study is indicated in Fig. 1. There were 25 high altitude balloon flights at various times in cycle XX and at different latitudes. The balloon flights provide the best altitude survey of environmental quantities. There were over three hundred airplane flights using RB57F, U2 and 707 aircraft. The aircraft provided detailed latitude surveys, balloon calibration rendezvous flights and flights during solar flare events. It is unfortunate that due to funds limitations, not all of the data was finally reduced and we could not continue the flight program through August 1972 when an extremely large solar event occurred. A more detailed description of the experiment is given by Foelsche[4] and Korff et al.[7]

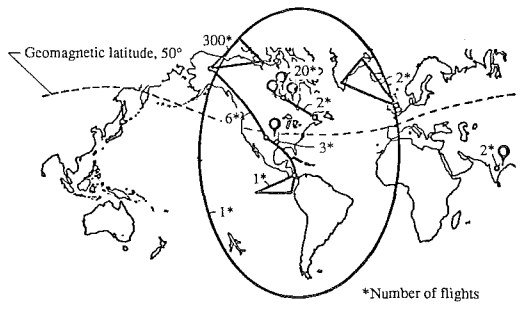

Figure 1. World map showing experimental flights with aircraft and balloons.

Radiation Levels at High Latitude

Figure 2 shows the measurements made on a high-altitude balloon flight during galactic cosmic ray maximum at 69° geomagnetic latitude. The instruments for this flight were only lightly shielded (less than 1 g cm^{-2} of fiber glass and foam for thermal insulation). The features to be noted in Fig. 2 are the broad maximum in the neutron flux, with peak at 60–70 millibars and the leveling off of the ion chamber dose rate above 50 millibars (1 mb $\approx$ 1 g cm^{-2}). Also shown is the present neutron model environment to be discussed and the model dose rate in tissue to be compared with the ion chamber data.

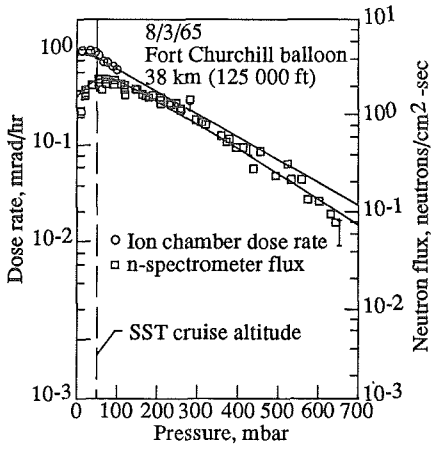

Figure 2. Galactic cosmic ray maximum (August 1965, 1 y after sunspot minimum, Fort Churchill, geomagnetic latitude $\approx$69°). Neutron fluxes in the range –10 MeV (right scale) and ion chamber dose rates (left scale) as a function of altitude.

In Fig. 3 are plotted data from a flight out of Fort Churchill in a period of increased solar activity, which is typical for about 2 y after galactic cosmic ray maximum. The ion chamber dose rate and the neutron flux decreased by about the same percentage during the 2 y. These decreases are due to a corresponding increase of the scattering power of the interplanetary magnetic fields. The dotted line between 0 and 300 g cm^{-2} in Fig. 3 is the shape of the altitude profile of neutron intensities 1 to 10 MeV as obtained from the theoretical nucleon cascade calculations described by Wilson et al.[11–13] using the Bertini nuclear model.[14–15] The neutron flux and tissue dose rate of the present model environment are also shown.

Figure 4, is an example for the neutron dose determinations, the neutron spectrum from galactic cosmic rays measured in the range 1 to 10 MeV at SST altitude on 3 August 1965, above Fort Churchill is extrapolated to lower energies (0.01 MeV) and higher energies (500 MeV); the results of the Monte Carlo calculations are shown by the horizontal dashes, representing the neutron fluxes compiled in the corresponding energy bins. From this spectrum the dose and dose equivalent rates for hands and feet due to neutrons are obtained by summing the dose rates resulting from multiplying the flux in each energy interval by the corresponding flux-to-dose rate conversion factor for the extremities. The resulting dose rate is 1.23 μGy h^{-1} (0.123 mrad h^{-1}) and the corresponding dose equivalent rate is 7.72 μSv h^{-1} (0.772 mrem h^{-1}). In addition to the spectrum, the separate

contributions in the different energy ranges to the dose and dose equivalent rates are indicated in Fig. 4 (linear scale on left-hand side). The neutrons of energies greater than 10 MeV are found to contribute (through recoil protons and stars) 35% to the total dose equivalent rate of neutrons. The neutrons of energy 0.1 to 1 MeV, assumed to have an energy spectrum similar to that given by Newkirk[15] (a typical slowing spectrum), contribute about 27%. The unmeasured part of the spectrum thus contributes about 70% to the neutron dose equivalent rate in extremities. While the slowing down spectrum is firmly established the high energy neutron production spectrum is uncertain by 20%. The overall uncertainty in the neutron dose is about 14%.

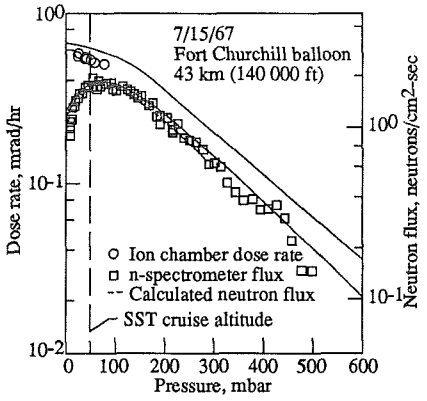

Figure 3. Galactic cosmic rays 2 y after galactic cosmic ray maximum (July 1967, Fort Churchill, geomagnetic latitude ≈69°). Compare with Fig. 2 for a flight at galactic cosmic ray maximum. The neutron flux and ion chamber dose rate have both decreased about 25–30% at SST altitudes (solar modulation). The solid line is the altitude dependence obtained by theory (Foelsche et al. 1974).

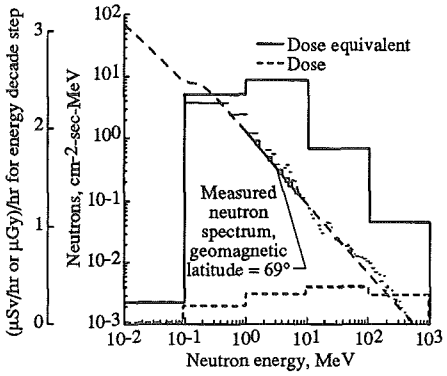

Figure 4. The high-latitude (geomagnetic latitude ≈69°) neutron spectrum measured at SST altitudes (≈50 g cm^{-2}) on 3 August 1965 (heavy solid line between 1 and 10 MeV) by Korff et al. (1979), with its extension to lower and higher energies (heavy dashed curve) compared with the shape of the Monte Carlo spectrum (histogram, horizontal dashes). The right-hand linear scale is for the dose rates in extremities calculated from the NASA spectrum (rem — heavy step curve; and rad — dashed step curve).

The main results of these measurements on galactic cosmic rays are the determinations of the absolute values of the energetic secondary neutron fluxes (1 to 10 MeV) and of their flat spectrum, which were in doubt before the present experiments, especially for high latitudes and altitudes, and the measurements with tissue equivalent ion chambers, which also yielded the contributions of neutrons (via recoil protons) to the absorbed dose in tissue, which is not obtained in conventional metal-walled ion chambers.

The theoretical spectra have as yet to be normalized by adjusting the absolute intensities to the measured neutron spectra in the 1 to 10 MeV range. The theoretical spectra are based on calculations for proton primaries and do not accurately take into account the α-particles and heavier nuclei that are present in galactic and solar cosmic rays, because the secondary production cross sections in reactions with air have not been satisfactorily determined either theoretically or experimentally. For the present purposes, it is considered satisfactory to assume that only the intensity and not the shape of the neutron spectra at subsonic and supersonic jet altitudes is substantially changed by the heavier primaries.

Radiation Levels Within the Geomagnetic Field

The latitude surveys were mostly made by aircraft so that the relation between aircraft countrates and balloon countrates need to be established (effect of neutron production and moderation by the aircraft structure). The aircraft countrates are found to be 10% higher in balloon rendezvous flights with identical instruments as well as within the solar cycle for the same instrument.[7] The latitude surveys by balloon and aircraft are shown in Fig. 5 at the transition maximum and at 250 g cm^{-2} for different phases of solar cycle XX. The curves in the figure are our approximation to the data given by

$$\begin{aligned}\phi_{1-10}(x_m, R, C) = 0.23 &+ [1.1 + 0.167(C - 100)]e^{-R^2/81} \\ &+ [0.991 + .0501(C - 100) \\ &+ 0.4\, e^{(C-100)/3.73}]\, e^{-R^2/12.96}\end{aligned} \quad (1)$$

at the transition maximum and

$$\begin{aligned}\phi_{1-10}(250, R, C) = 0.17 &+ [0.787 + 0.035(C - 100)]e^{-R^2/25} \\ &+ [-.107 - 0.0265(C - 100)] \\ &+ 0.612e^{(C-100)/3.73}]\, e^{-R^2/139.2}\end{aligned} \quad (2)$$

at 250 g cm^{-2} depths in the atmosphere where R is local cutoff rigidity (GV) and C is the high latitude neutron monitor count rate in percent of maximum. At depths below 250 g cm^{-2}, the neutrons attenuate with attenuation length (g cm^{-2}) given by

$$\lambda = 165 + 2R \quad (3)$$

The flux at all altitudes is approximated as

$$\phi_{1-10}(x, R, C) = f(R, C)e^{-x/\lambda} - F(R, C)e^{-x/\Lambda} \quad (4)$$

where

$$f(R, C) = e^{250/\lambda}\, \phi_{1-10}\,(250, R, C) \quad (5)$$

$$\Lambda = \lambda \left[1 - \frac{\phi_{1-10}(x_m, R, C)e^{x_m/\lambda}}{f(R, C)}\right] \quad (6)$$

and

$$F(R,C) = \frac{\Lambda}{\lambda} f(R,C) e^{x_m/\Lambda - x_m/\lambda} \quad (7)$$

where the transition maximum altitude corresponds to

$$x_m = 50 + \ln\left[2000 + e^{-2(C-100)}\right] \quad (8)$$

The neutron environment model given by eqn. (1) to (8) is shown in Figs. 2 and 3 in comparison to the experimental data. The 1-10 MeV flux is converted to dose equivalent and dose rates using 3.14 μSv-cm^2-s-h^{-1} (0.314 mrem-cm^2-s-h^{-1}) and 0.5 μGy-cm^2-s-h^{-1} (0.05 mrad-cm^2-s-h^{-1}), respectively.

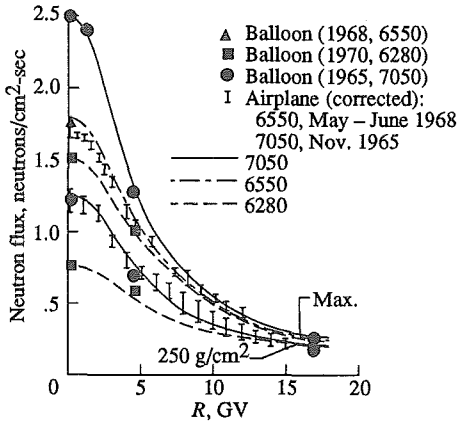

Figure 5. Neutron flux from latitude surveys as a function of Deep River neutron monitor count rate.

Unfortunately, not all of the ion chamber data nor the nuclear emulsion data were reduced. For our present purpose we will use the argon-filled ion chamber data to represent the altitude, latitude and solar cycle dependence and use the available tissue equivalent ion chamber data as a guide. The ion chamber data compiled by S. B. Curtis[16] is shown in Table 1 for solar minimum ($C = 98.3$, 1965) and in Table 2 for solar maximum ($C = 80$, 1958) as obtained for cycle XIX. We note that the low energy GCR had not fully recovered in the summer of 1965 so the high latitude ionization at high altitude is about 10% lower than in 1954. Furthermore the 1958 measurements near solar maximum covered only mid to high latitudes and the low latitude data in Table 2 is likely to be about 10% too high at high altitudes. The ionization rates in Tables 1 and 2 are the rates in air per atmosphere of pressure. They are directly converted to exposure units and absorbed dose in tissue. The comparison to the tissue equivalent ion chamber requires the addition of the neutron absorbed dose rates as shown in Figs. 2 and 3 where good consistency between the two methods is demonstrated. Dose equivalent requires an estimate of the high LET components associated with charged particles and are found from the measurements in nuclear emulsion. The corresponding average quality factor for proton produced stars is found from Davidson's emulsion data as

$$Q_F = 1. + .35e^{-x/416} - .194e^{-x/65} \quad (9)$$

This average quality factor will be applied to ion chamber dose rate data to account for charged particle induced stars in tissue.

Comparison to Others

This first comparison is with the dose equivalent rate meter of the Brookhaven National Laboratory (BNL). The BNL instrument is a tissue equivalent spherical proportional counter of 22 cm radius filled at 10 torr with tissue equivalent gas (corresponds to a 3 μm tissue site). The LET spectra is derived using the triangular relation to lineal energy which assumes the chamber size is small compared to the range of the particles being detected.[17] The ICRP-26 quality factor[5] is used to calculate dose equivalent rates. Due to the large chamber size at the chosen pressures, the high LET events are distorted by the triangular assumption.

Table 1. Ionization rates in air measured by argon filled chambers[a] at solar minimum ($C = 98.3$, 1965).

	Ion pairs (cm^{-3} s^{-1}) at air depth (g cm^{-2}) of													
R(GV)	30	40	50	60	70	80	90	100	120	140	200	245	300	1034
0	445.0	430.0	414.0	399.0	383.0	366.0	349.0	332.0	298.0	266.0	181.0	136.0	95.0	11.4
.01	445.0	430.0	414.0	399.0	383.0	366.0	349.0	332.0	298.0	266.0	181.0	136.0	95.0	11.4
.16	444.0	430.0	414.0	399.0	383.0	366.0	349.0	332.0	298.0	266.0	181.0	136.0	95.0	11.4
.49	411.8	404.3	394.4	382.0	369.0	354.8	339.4	325.0	292.3	264.5	181.0	136.0	95.0	11.4
1.97	325.0	333.0	340.0	335.0	330.0	312.5	308.0	300.0	285.0	264.0	181.0	134.0	95.0	11.4
2.56	300.0	305.0	310.0	305.0	300.0	290.0	285.0	280.0	255.0	230.0	173.0	126.0	95.0	11.4
5.17	185.0	195.0	208.0	208.0	208.0	208.0	208.0	208.0	195.0	185.0	135.0	103.0	75.0	10.6
8.44	127.6	137.0	145.0	150.2	153.8	155.8	156.0	154.6	149.7	142.2	111.3	87.0	66.6	10.4
11.70	85.0	92.0	98.0	100.0	102.0	105.0	107.0	110.0	108.0	105.0	80.0	77.0	60.0	10.0
14.11	70.0	75.0	82.0	85.0	89.0	93.6	95.0	100.0	98.0	95.0	78.0	68.8	50.0	10.0
17.00	66.3	73.8	80.0	84.8	88.5	91.1	92.6	93.5	93.4	90.5	75.0	62.3	48.0	10.0

[a]Experimental data extrapolated to provide estimates of ionization rates over a wide range of altitudes and geomagnetic cutoffs.

Table 2. Ionization rates in air measured by argon filled chambers[a] at solar maximum ($C = 80$, 1958).

	Ion pairs (cm^{-3} s^{-1}) at air depth (g cm^{-2}) of													
R(GV)	30	40	50	60	70	80	90	100	120	140	200	245	300	1034
0	264.6	267.5	267.0	265.0	258.0	252.0	243.0	235.0	216.3	197.0	145.0	109.2	78.8	11.4
.01	264.6	267.8	267.0	265.0	258.0	251.0	243.0	235.0	216.3	197.0	145.0	109.2	78.8	11.4
.16	264.0	264.9	265.0	264.0	257.0	250.0	243.0	233.0	215.0	197.0	145.0	109.2	78.8	11.4
.49	264.0	264.9	265.0	262.0	256.0	249.0	242.0	231.0	213.2	197.0	145.0	109.2	78.8	11.4
1.97	264.0	265.0	265.0	262.0	252.0	245.0	241.0	231.0	212.5	197.0	145.0	107.8	78.8	11.4
2.56	235.0	237.5	240.0	240.0	239.0	238.0	237.0	230.0	209.0	197.0	145.0	101.6	78.8	11.4
5.17	162.5	168.0	179.0	182.0	178.0	175.2	174.0	173.8	170.0	160.0	159.0	88.3	65.0	10.6
8.44	95.0	103.5	112.0	118.0	118.0	119.0	120.0	122.0	118.0	117.0	100.6	78.7	60.2	10.4
11.70	78.2	85.0	90.7	92.7	94.8	98.0	100.0	103.1	101.2	98.4	75.0	72.2	56.2	10.0
14.11	65.7	70.7	77.5	80.5	84.3	89.0	90.5	95.3	93.5	90.9	74.0	65.9	47.9	10.0
17.0	63.0	70.3	76.4	81.1	84.8	87.5	89.1	90.2	90.1	87.4	72.6	60.3	46.5	10.0

[a]Experimental data extrapolated to provide estimates of ionization rates over a wide range of altitudes and geomagnetic cutoffs.

Table 3. Radiation measurements of the BNL instrument compared to present model (values in parentheses).

Geomagnetic Latitude (°N)	Date	Altitude (km)	Areal density (g cm^{-2})	Absorbed-Dose Rate (μGy h^{-1})	Dose-Equivalent Rate (μSv h^{-1})
36.7	29 Aug 1972	3.0	694	0.18 (0.18)	0.25 (0.30)
	DRNM $\simeq$ 6950	6.1	460	0.58 (0.57)	1.00 (1.12)
		9.1	303	1.38 (1.21)	2.50 (2.55)
		12.2	188	2.80 (2.32)	4.75 (4.82)
41.7	30 Aug 1972	3.0	694	0.20 (0.19)	0.25 (0.36)
	DRNM $\simeq$ 6950	6.1	460	0.63 (0.59)	0.88 (1.29)
		9.1	303	1.50 (1.28)	2.45 (2.99)
		12.2	188	3.10 (2.57)	5.25 (5.76)
50.0	17 Jun 1972	3.0	694	0.22 (0.20)	0.35 (0.43)
	DRNM $\simeq$ 6950	6.1	460	0.61 (0.69)	1.05 (1.63)
		9.1	303	1.68 (1.59)	2.75 (3.95)
		12.2	188	3.45 (3.14)	5.80 (7.61)
58.0	18 Jul 1972	3.0	694	0.19 (0.20)	0.42 (0.45)
	DRNM $\simeq$ 6950	6.1	460	0.63 (0.69)	1.21 (1.72)
		9.1	303	1.70 (1.59)	2.90 (4.25)
		12.2	188	3.90 (3.35)	7.00 (8.52)
69.4	29 Jun 1971	9.1	303	1.59 (1.57)	2.34 (4.09)
69.6	DRNM $\simeq$ 6850	11.6	204	2.88 (2.97)	4.89 (7.53)
68.4		15.2	116	4.89 (4.97)	7.93 (12.09)
67.3		18.3	71	6.03 (6.14)	10.39 (14.24)

For example, a 100 keV μm^{-1} proton moving along the diameter would register only a 75 keV pulse instead of the 300 keV pulse as expected using the assumptions leading to the triangular distribution. The instrument assigned quality factor would be 10 instead of the correct value of 20. Such distortions are *worse* for multiple charged ions produced as nuclear fragments of the tissue material.[18] Such fragments are known to be important in predicting biological response.[19] Theeefore the BNL instrument could significantly underestimate the average quality factor. With this limitation in mind we give the BNL measurements made in 1971 and 1972 in Table 3 along with results of the present model. Approximate neutron monitor countrates used in evaluating the present model are given for the Deep River neutron monitor (DRNM). The dose rates are in quite good agreement but the quality factors of the present model are substantially larger than the values measured by the BNL instrument. The largest is at the highest latitudes and will be discussed further subsequently.

The present model is compared to several sources in Table 4. Of particular note is the result of Schaefer's measurements with nuclear emulsion.[20] In particular, the ionization tracks of all particles *other than* nuclear stars leads to 5.8 μGy h^{-1} and 10.5 μSv h^{-1}, respectively, in good

Table 4. Present results compared with other estimates of galactic radiation dose-equivalent rate (μSv h^{-1}).

Source of Data	Altitude (areal density)	
	11.0 km (255 g cm^{-2})	18.3 km (71 g cm^{-2})
	At or near 55°N, solar average (DRNM = 6,660)	
Present	5.9	12.1
O'Brien-McLaughlin	4.1	13.2
LRC Extremities	6.2	12.5
	42°, 43°N, at or near solar maximum (DRNM = 6,950)	
Present	4.8	8.6
O'Brien-McLaughlin	3.3	9.8
BNL	3.9	—
	67°–70°N, at or near solar maximum (DRNM = 6,850)	
Present	6.7	14.2
BNL	4.1	10.4
Concorde	—	8.0
HARIS	—	9.0
Schaefer	—	15.0

agreement with the BNL instrument 6.0 μGy h^{-1} and 10.4 μSv h^{-1} as given in Tables 3 and 4. The nuclear star contributions from Schaefer's nuclear emulsion data gives final values of 6.5 μGy h^{-1} and 15.0 μSv h^{-1} in excellent agreement with the present model of 6.1 μGy h^{-1} and 14.2 μSv h^{-1}. The importance of the nuclear star contribution (the highest LET components) has also been noted by Friedberg and Neas.[20] The present model appears in excellent agreement with measurements which include the high LET components associated with nuclear star contributions.

Global Dose Rate Estimates

The dose rate evaluation methods described herein are directly applicable to predictions, or estimates, of global dose and dose equivalent rate patterns. The requirements for such an analysis include the geographic distribution of magnetic cutoff values and the global pressure fields at the altitudes of interest. The vertical geomagnetic cutoff values are taken here as the 1980.0 epoch data of Shea and Smart[21] and are shown in Fig. 6. The atmospheric climatological data have been extracted from the Langley Research Center General Circulation Model (LaRC-GCM) of the Earth's atmosphere.[22,23] For purposes of computations presented herein, the original latitude-longitude grid has been reduced to 10-degree increments by appropriate interpolation of the LaRC-GCM data; i.e., the latitude grid points are −90° to +90°, and the longitudes progress from −180° to +180° in 10° steps.

Pressure distribution at 14 km altitude is shown in Fig. 7. The pressure distribution is shown in polar stereographic projection for both hemispheres and for both solstice conditions. The northern hemisphere winter solstice (southern hemisphere summer) has been modeled as an average of pressure for the first 10 d in January as given by the LaRC-GCM. The corresponding opposite solstice conditions are represented by an average of the data for the first 10 d in July. Pressure contours are given in mbar. (Note that, for the Earth's atmosphere, pressure in mbars p is numerically within 2% of the overhead absorber amount x in units of g cm^{-2} as is required in equations (1)–(9).) Some general salient features of the pressure distributions may be noted; for example, the equator-to-pole latitudinal gradient is much larger for each hemisphere during winter than in summer. As a consequence of this, substantial seasonal variation in dose rates may result, particularly for high latitude flights in the northern hemisphere.

Contour maps of the dose rate at solar minimum corresponding to the 14 km altitude level is presented in Fig. 8. Dose rate values for the contours are expressed in units of mSv per 1,000 h. The dose rate increases from low latitudes by approximately a factor of three as polar regions are approached. At the 18-km height ($\sim$ 60,000 ft), the equator-to-pole increase is on the order of a factor of 5, due largely to the increasing influence of the geomagnetic cutoffs relative to the atmospheric attenuation. Note that even for the 14-km altitude, dose rates at high latitudes in the polar winter are greater than 10 mSv per 1,000 h. Such regions of the globe in the northern hemisphere encompass

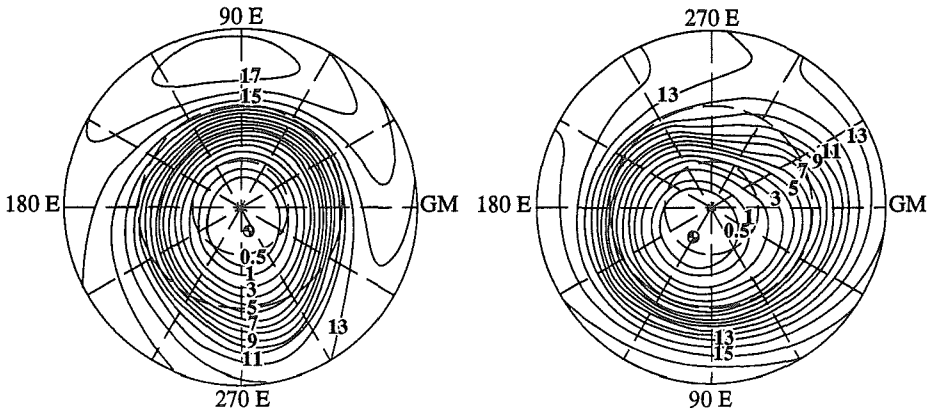

Northern hemisphere

Southern hemisphere

(a) New York – Tokyo

(b) New York – London

Figure 6. Contour of vertical geomagnetic cutoff values from data of Shea and Smart (1983). Contour increments are 1 GV except for the lowest (0.5 GV) contour. Magnetic pole locations are indicated.

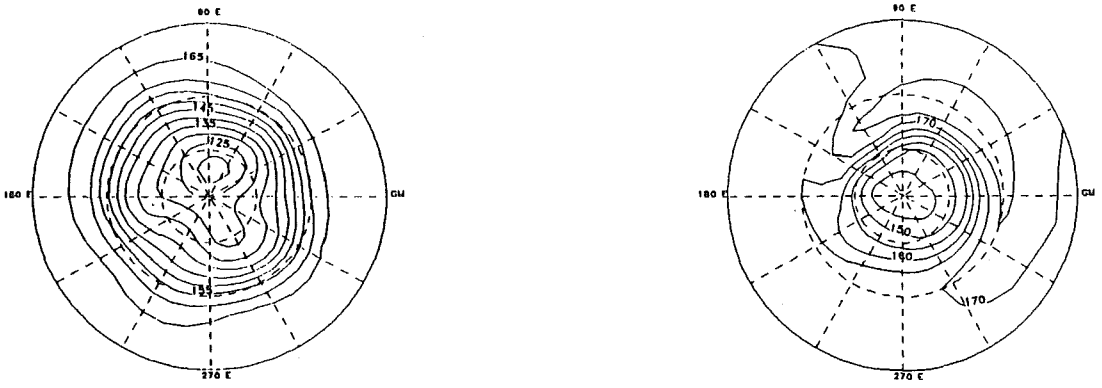

(a) Northern hemisphere winter (Jan. data).

(b) Northern hemisphere summer (July data).

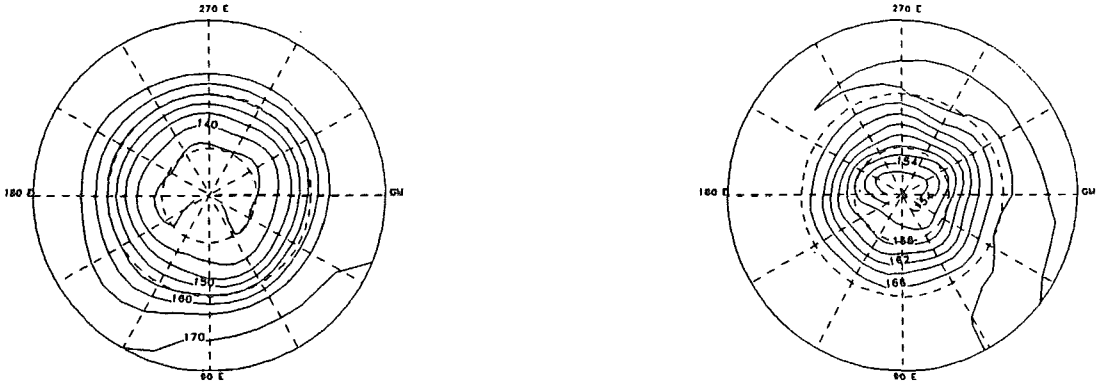

(c) Southern hemisphere winter (July data).

(d) Southern hemisphere summer (Jan. data).

Figure 7. Global pressure distribution for solstice conditions at 14 km (approx. 46,000 ft.). Contour values are in mbar units.

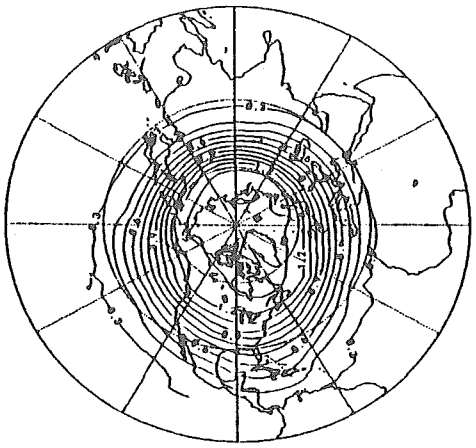

(a) Northern hemisphere winter (Jan. data).

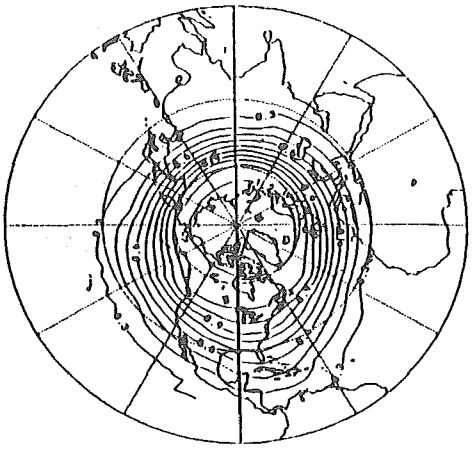

(b) Northern hemisphere summer (July data).

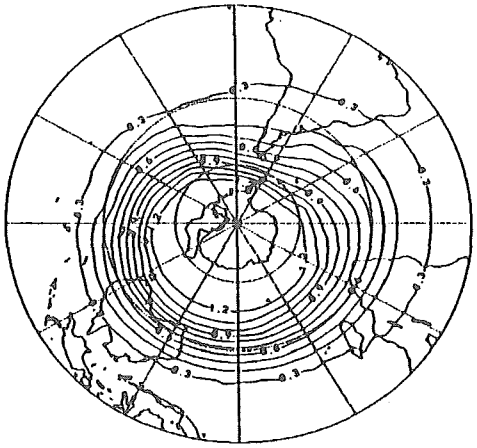

(c) Southern hemisphere winter (July data).

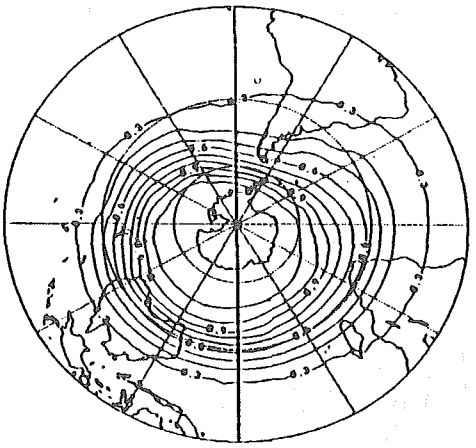

(d) Southern hemisphere summer (Jan. data).

Figure 8. Contours of dose rate during solstice conditions at 14 km (approx. 46,000 ft.) computed with ICRP-26 (1977) quality factor. Contour increment is 1 mSv per 1,000 h.

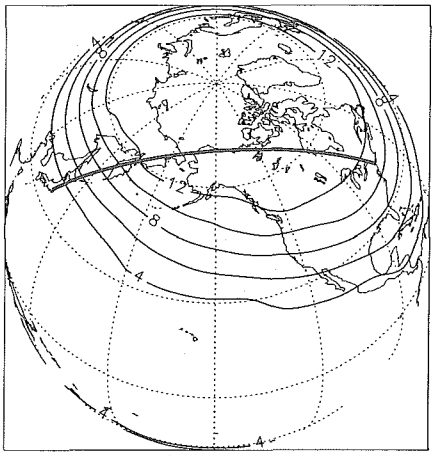

(a) New York – Tokyo

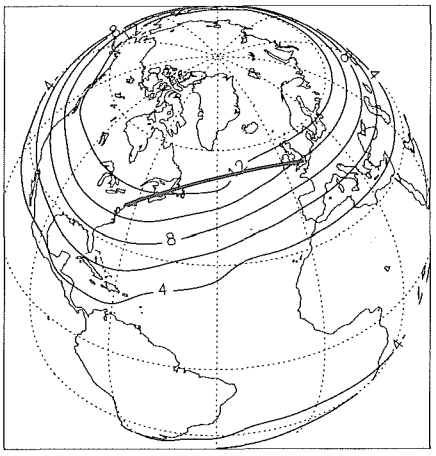

(b) New York – London

Figure 9. International great circle routes for northern hemisphere winter at 14 km. Dose rates contours are computed with factor ICRP-26 (1977) quality factor and in mSv per 1,000 h.

several common international flight paths. Two such routes (N.Y.-London and N.Y.-Tokyo) are indicated in Fig. 9 which have been overlaid on satellite-view projections of the globe showing contour maps of the northern hemisphere winter dose rate at the 14-km level. The average dose rate for the flight path is found by averaging over the contours.

A computer program has been written to generate the worldwide atmospheric radiation exposure as a function of latitude, longitude, altitude, neutron monitor countrate and time within the calendar year. A menu driven main program calculates the average exposure rate between arbitrary origination and destination points assuming flight along the great circle at any specified altitude. The program could be easily modified to simulate any flight trajectory.

Revised Quality Factors

All of the previous results were based on the quality factors of ICRP-26.[5] Average neutron quality factors have been derived using the proposed ICRP-60[2] quality factors and will be used here to estimate expected future upward revisions. The contributions to neutron dose equivalent rates in neutron energy subintervals as presented in Fig. 4 are shown in the first three columns of Table 5. The corresponding previous average quality factors for each subinterval are shown in column four. The newly recommended quality factors (ICRP-60) are averaged over each subinterval according to the neutron spectrum produced by GCR and then applied to obtain new estimates of the neutron dose equivalent rates, as shown in columns five and six. The results change the neutron dose equivalent by 45%. In that the assumed quality factor of 20 is a generous overestimate of nuclear star contributions to dose equivalent,[19,24] we do not increase the charged particle star contribution.

Table 5. Dose (ΔD, μGy h^{-1}) and dose equivalent (ΔH, μSv h^{-1}) rates in neutron energy intervals (ΔE, MeV) with the ICRP-26 (1977) and the new ICRP-60 (1991) quality factors (Q).

ΔE	ΔD	ΔH_{26}	Q_{26}	Q_{60}	ΔH_{60}
0.1–1	.20	2.34	11.7	20.	4.0
1–10	.32	2.52	7.9	13.5	4.32
10–100	.39	1.81	7.0	7.0	1.81
100–1,000	.31	1.04	3.4	3.4	1.04
.1–1,000	1.22	7.71	6.3	9.2	11.17

International flights for New York-London and New York-Tokyo are shown in Fig. 10 at solar minimum during winter solstice for 14 km altitudes. Such flights will accumulate more than 15 mSv per 1,000 h. Clearly high exposures relative to the general public are indicated and some thought to possible crew rotation (especially for potentially pregnant crew members) seems advisable even for the current exposure limit of 5 mSv during gestation. It appears that some crew counciling will be in order if the newly proposed quality factors are in fact adopted.

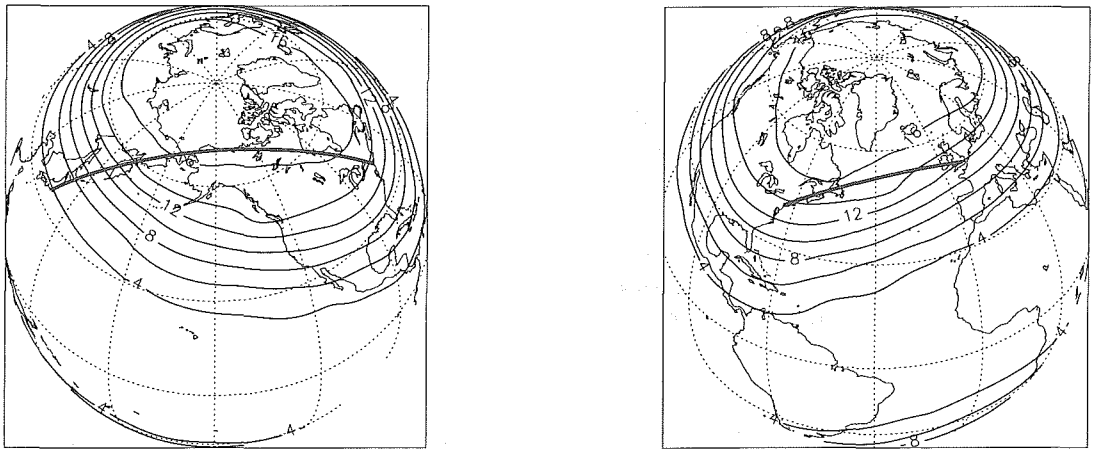

(a) New York – Tokyo

(b) New York – London

Figure 10. International great circle routes for northern hemisphere at 14 km. Dose rate contours are computed with ICRP-60 (1991) quality factor and are in units of mSv per 1,000 h.

Analysis For Selected Flight Paths

The environmental model described previously is used in conjunction with the background radiation data base to estimate rates of incurred dose equivalent for several intercontinental and domestic routes at three altitudes (12, 14,and 17 km, corresponding approximately to 40,000, 46,000 and 56,000 ft, respectively). Several tables of results have been prepared (Tables 6–8) in which the predicted average dose rates are presented for the selected flight paths for various input parameters. The routes are specified as minimum distance (great circle) routes at constant altitude.

Dose equivalents for 950 block hours for the average of cycle XX and medium season for several city pairs and altitudes used in a recent FAA circular are shown in Table 6. Also shown are the values from the O'Brien-McLaughlin theory as presented in the FAA circular. Generally, the

FAA results are a few to 13% higher than present values except for the N.Y.-Athens flight. It is difficult for us to understand why the midlatitude flight such as N.Y.-Athens should receive a much higher exposure than the N.Y.-Tokyo flight which passes within several degrees of the magnetic north pole (see Fig. 10). As a check on our code we chose a route similar to the N.Y.-Athens city pair but lying further north and used a much higher altitude shown as the Boise-Baghdad city pair for which 8.42 mSv was obtained for solar minimum in the winter. Clearly, the 9.1 mSv for N.Y.-Athens appears high.

Table 6. Dose equivalent for 950 block hours.

Conditions: Solar cycle XX ave., DRNM ≈ 6,668.
QF: ICRP-26 (1977)
Season: April

City pairs	Altitude, km (kft)	Dose, mSv	
		Present	FAA
N.Y.– Tokyo	13.1 (43)	6.75	7.0
N.Y.– Seattle	11.9 (39)	6.00	6.5
N.Y.– London	11.9 (39)	6.08	6.9
Chicago– London	11.9 (39)	6.33	7.1
N.Y.– Athens	12.5 (41)	5.85	9.1
Boise– Baghdad	39.6 (130)	8.42[a]	—

[a]Winter solstice at solar minimum.

Table 7 gives results computed for solar minimum and northern hemisphere winter and summer conditions. The ICRP-60 quality factor result in dose equivalent values are higher by 25 to 33%, with largest increases for the higher latitude routes. In order to examine the effect of active Sun conditions for these proposed quality factors, Table 8 has been generated for the solar maxima of cycles XIX and XX in which the relative solar activity is known to have an inverse relationship to the Deep River neutron monitor count rate. It is seen that the decrease in dose rate during solar maximum may be quite large, especially at high latitudes. For example, the average rates at all altitudes considered for the N.Y.-Tokyo route are reduced during the cycle XIX maximum to almost half the predicted quiet Sun values (Table 7 vs. 8). Comparison of the values in Table 8 for different solar maxima indicate that effects of variabilities between different cycles can be significant. Clearly, much larger temporal variations are observed in the atmosphere than the 9–15 percent given by the O'Brien-McLaughlin theory.[25]

As a final illustration of the range of dose rate variation along particular flight paths, the calculated dose equivalent rate at 17 km altitude for N.Y.-Tokyo and for Paris-Rio de Janeiro are shown as a function of distance traveled in Fig. 11. The dose rate for N.Y.-Tokyo is in excess of 15 mSv per 1,000 h since much of the route is at high latitudes (>50°N). In contrast, the Paris-Rio calculation, for which most time is spent at tropical and sub-tropical latitudes, shows much lower dose rates. The average dose rate for the more northern route exceeds that of the low-latitude route by more than 2-1/2 times.

It may be noted that in the preceding, dose-equivalent rates have been expressed in mSv per 1,000 h. If one assumes that crew-members spend 1,000 h per year at altitude, the tabular results convert directly to annual incurred dose. When such a conversion is made, it is noteworthy that only the flight path at equatorial latitudes (Paris-Rio) is determined to be within the currently accepted 5 mSv annual limit for the general populace. The more northerly routes, especially at high altitudes, are often in excess of this limit by factors of 2 and sometimes 3 if the proposed increase in quality factors are in fact accepted.

Table 7. Dose equivalent rate, mSv per 1,000 h.

Conditions: Solar cycle min, DRNM = 7,157.
QF: ICRP-60 (1991)
Season: January (July)

City pairs	Dose equivalent rate at altitude of—		
	12,000 m (39,370 ft)	14,000 m (45,932 ft)	17,000 m (55,774 ft)
N.Y.– Tokyo	10.2 (8.6)	12.9 (11.6)	15.2 (14.8)
N.Y.– London	11.5 (9.7)	14.6 (13.2)	17.1 (16.7)
N.Y.– Athens	9.4 (8.0)	12.0 (10.8)	14.0 (13.6)
N.Y.– Seattle	11.3 (9.6)	14.7 (13.2)	17.5 (17.1)
Paris– Rio	3.7 (3.5)	4.6 (4.4)	5.4 (5.3)
Paris– D.C.	11.0 (9.3)	14.0 (12.7)	16.4 (16.0)
Atlanta– L.A.	7.4 (6.5)	9.6 (8.9)	11.5 (11.3)
Atlanta– N.Y.	9.4 (8.1)	12.2 (11.1)	14.6 (14.3)
Atlanta– S.F.	8.0 (7.0)	10.4 (9.5)	12.4 (12.2)
Chicago– London	11.9 (10.1)	15.1 (13.7)	17.9 (17.4)
L.A.– London	11.2 (9.7)	14.3 (13.1)	17.1 (16.7)

Table 8. Dose Equivalent Rate, mSv per 1,000 h.

Conditions: Solar cycle XX max (Solar cycle XIX max)
QF: ICRP-60 (1991)
Season: January

City pairs	Dose equivalent rate at altitude of—		
	12,000 m (39,370 ft)	14,000 m (45,932 ft)	17,000 m (55,774 ft)
N.Y.– Tokyo	7.1 (6.0)	9.1 (7.3)	10.6 (8.2)
N.Y.– London	7.9 (6.6)	10.1 (8.1)	11.9 (9.2)
N.Y.– Athens	6.9 (6.0)	8.7 (7.3)	10.2 (8.2)
N.Y.– Seattle	7.7 (6.3)	10.1 (8.0)	12.1 (9.3)
Paris– Rio	3.3 (3.3)	4.1 (3.9)	4.8 (4.4)
Paris– D.C.	7.7 (6.5)	9.9 (8.0)	11.6 (9.1)
Atlanta– L.A.	5.9 (5.6)	7.6 (6.9)	9.1 (7.8)
Atlanta– N.Y.	6.8 (6.0)	8.9 (7.6)	10.8 (8.8)
Atlanta– S.F.	6.2 (5.8)	8.1 (7.2)	9.6 (8.1)
Chicago– London	8.1 (6.6)	10.4 (8.1)	12.2 (9.3)
L.A.– London	7.8 (6.4)	9.9 (7.9)	11.8 (9.0)

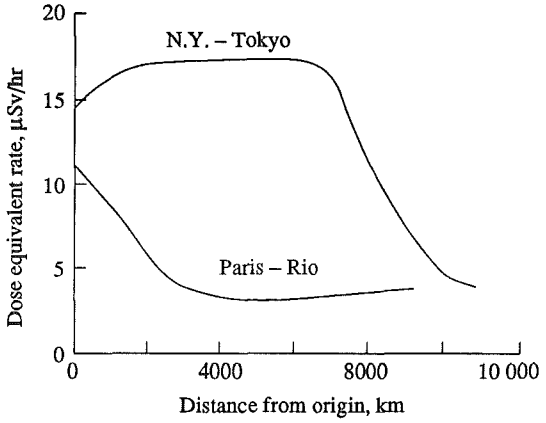

Figure 11. Dose equivalent rate profile along the aircraft flight trajectories at 17 km (56,000 ft).

Revised Radiation Limits

In addition to the upward revision of the recommended quality factor, the recommended exposure limits have been substantially reduced.[2] Although the annual limit for radiation workers is still 50 mSv, an additional limit of not more than 100 mSv in any five years is given. These limits are not expected to be exceeded by the current background exposures for flight times of 1,000 hours per year or less. A more difficult requirement is to limit the exposure of pregnant workers. The allowable exposure for the unborn child is 2 mSv during gestation. Such an exposure could be achieved in 2 months for even some domestic U.S.A. flights. A flight crew member could reach the maximum allowable even before pregnancy is hardly detected. Even then exposure records would be required to provide adequate counciling and career planning. We emphasize that such measures seem only warranted if the revised quality factors and dose limits are accepted as regulatory standards. If exposure records are required, then the present model (computer code) would be helpful in establishing such records and for counciling of airline workers in choosing flight schedules. Such conclusions are exclusive of the possibility of a large solar flare which must be reconsidered.[4]

The measured data of the present report are all within 10 percent accuracy. This leaves the extrapolated neutron spectrum as the main uncertainty. The slowing down spectrum is well known but the high energy neutron spectrum based on the proton-neutron intranuclear cascade model has an inherent 20 percent uncertainty. Considering that about 60–70 percent of the neutrons are produced by incident protons at the top of the atmosphere and that the heavy ion produced neutron spectrum may be substantially different, the high energy neutron spectrum is probably the greatest uncertainty in the present model. Most important in the experimental study of high energy neutrons would be latitude surveys at high altitudes since the proton to heavy ion ratio is greatest near the magnetic poles and is substantially reduced near the equator.

Acknowledgement

The authors extend their warm appreciation to Dr. S. B. Curtis of the Lawrence Berkeley Laboratory for allowing us to use his compilation of atmospheric ionization data and useful discussions in the course of this work.

References

1. W. K. SINCLAIR, "Recent Developments in Estimation of Cancer Risk From Ionizing Radiation," Warrendale, PA: Engineering Society for Advanced Mobility Land, Sea, Air and Space; SAE Technical Paper 901344; 1990.
2. International Commission on Radiological Protection. Recommendations of the ICRP. Oxford: Pergamon Press; ICRP Publication 60, Ann. ICRP 21(1–3); 1991.
3. EUGENE NORMAND, J. L. WERT, W. R. DOHERTY, D. L. OBERG, P. R. MEASEL, and T. L. CRISWELL, "Use of PaBe Source to Simulate Neutron-Induced Single Event Upsets in Static RAMs," IEEE Trans. on Nucl. Sci., 35, 1523 (1988).
4. T. FOELSCHE, , R. B. MENDELL, J. W. WILSON, and R. R. ADAMS, "Measured and Calculated Neutron Spectra and Dose Equivalent Rates at High Altitude; Relevance to SST Operations and Space Research." Washington, DC: NASA; NASA TN D-7715; 1974.
5. International Commission on Radiological Protection. Recommendations of the ICRP. Oxford: Pergamon Press; ICRP Publication 26; Ann. ICRP 1(3); 1977.
6. W. DAEHNICK, R. SHERR, "Pulse Shape Discrimination in Stilbene Scintillators," Rev. Sci. Inst. 23:666–670, 1961.
7. S. A. KORFF, R. B. MENDELL, M. Merker, S. LIGHT, H. J. VERSCHELL, W. S. SANDIC, "Atmospheric Neutrons," Washington, DC. NASA CR-3126; 1979.
8. R. J. A. KURZ, "709/7090 Fortran II Program to Compute the Neutron-Detection Efficiency of Plastic Scintillator for Neutron Energies from 1 to 300 MeV." UCRL-1139, 1964.
9. M. F. SCHNEIDER, "Advanced Spaceborne Dosimetry Instrumentation," WL-TDR-64-96, U.S. Air Force, Dec. 1965.
10. M. F. SCHNEIDER, J. F. JANNI, and G. C. AINSWORTH, "Operational Radiation Instrumentation and Flight Crew Dosimetry for the Skylab Program," In:

Warman, E. A., ed. Proceedings of the national symposium on natural and manmade radiation in space. NASA TMX-2440, pp. 958–973, 1972.

11. J. W. WILSON, J. J. LAMBIOTTE, T. FOELSCHE, and T. A. FILIPPAS, "Dose Response Functions in the Atmosphere Due to Incident High Energy Protons Protection With Application to Solar Proton Events," Washington, DC: NASA; NASA TN D-6010; 1972.
12. J. W. WILSON, J. J. LAMBIOTTE, and T. FOELSCHE, "Structure in the Fast Spectra of Atmospheric Neutrons," J. Geophys. Res. 74:6494–6496; 1969.
13. J. W. WILSON, "Production and Propagation of Atmospheric Neutrons," Trans. Am. Nucl. Soc. 15:969–970; 1972.
14. H. W. BERTINI, "Preliminary Data From Intranuclear-Cascade Calculation of 0.75-, 1-, 2-GeV Protons on Oxygen, Aluminum and Lead and 1-Gev Neutrons on the Same Elements," Oak Ridge, TN: ORNL-TM-1996; 1967.
15. L. L. NEWKIRK, "Calculation of Low-Energy Neutron Flux in the Atmosphere by S_n Method," J. Geophys. Res. 68:1825–1833; 1963.
16. Boeing Co. Computation of Galactic Cosmic Radiation Exposure During Aircraft Flights. Seattle, WA: Document No. DGA 11471-1, Prepared by R. L. Swanson; 1969.
17. International Commission on Radiation Units and Measurements. The quality factor in radiation protection. Bethesda, MD: ICRU; ICRU Report 40; 1986.
18. J. W. WILSON, F. A. CUCINOTTA, and F. HAJNAL, "Analytical Relationships of Nuclear Field and Microdosimetric Quantities for Target Fragmentation in Tissue Systems," Health Phys. 60:559–565; 1991.
19. J. W. WILSON, J. L. SHINN L. W. TOWNSEND, "Nuclear Reaction Effects in Conventional Risk Assessment for Energetic Ion Exposure," *Health Phys.*, 58:749–752; 1990.
20. W. FRIEDBERG and B. R. NEAS, "Cosmic Ray Exposure During Air Travel," Washington, DC: Federal Aviation Administration; FAA-AM-80-2; 1980.
21. D. F. SMART, and M. A. SHEA, "Geomagnetic Transmission Functions for a 400 km Altitude Satellite," *18th International Cosmic Ray Convergence—Conference Papers*, MG Sessions, Vol. 3. Tata Inst. of Fundamental Research (Colaba, Bombay), pp. 419–422; 1983.
22. W. T. BLACKSHEAR, W. L. GROSE, and R. E. TURNER, "Simulated Sudden Stratospheric Warming; Synoptic Evolution," Q. Jour. Roy. Met. Soc. 113:815–846; 1987.
23. W. L. GROSE, J. E. NEALY, R. E. TURNER, and W. T. BLACKSHEAR, "Modeling the Transport of Chemically Active Constituents in the Stratosphere," In: Viscont, G., ed. Transport processes in the middle atmosphere. Dordrecht: D. Reidel; 1987.
24. J. L. SHINN and J. W. WILSON, "Nuclear Reaction Effects in Use of Newly Recommended Quality Factor," Health Phyis. 61:415–419, 1991.
25. W. FRIEDBERG, D. N. FAULKNER, L. SYNDER, E. B. DARDEN, and K. O'BRIEN, "Galactic Cosmic Radiation Exposure and Associated Health Risks for Air Carrier Crewmembers," Aviat. Space Environ. Med. 60:1104–1108; 1989.